NEAR SOURCE ENERGY PARTITIONING FOR REGIONAL WAVES IN 2D AND 3D MODELS: EFFECTS FROM RANDOM FREE SURFACE SCATTERING

Xiao-Bi Xie, Thorne Lay, Ru-Shan Wu, and Yaofeng He

University of California, Santa Cruz

Sponsored by Air Force Research Laboratory

Contract No. FA8718-05-C-0021

ABSTRACT

Regional seismic phases (e.g., Pn, Sn, Pg, Lg) play an important role in global monitoring of low-yield underground nuclear tests. Numerous empirical observations have shown that regional phases hold the keys to small-event magnitude and yield estimation and to discrimination between small explosions and earthquakes. However, building a sound physical basis for the application of the empirical relationships requires detailed knowledge of the regional phases (e.g., relative intensity and frequency dependence of different phases excited by earthquakes and explosions) and relationships linking the wave characteristics with a range of source and structure parameters. The complex excitation and energy-partitioning mechanisms yielding regional phases are difficult to empirically separate by data analysis. Thus, numerical modeling approaches are valuable for investigating excitation and propagation of regional seismic phases.

We use the 2D P-SV boundary-element simulation and the embedded array local slowness analysis method to investigate the effect of topographic scattering on the near-source energy partitioning for an explosion source. Random topographic models with different statistical properties, variable source depth, and different Q models are investigated using numerical simulations. With this method, the responses of different phases as functions of frequency and source/model parameters are calculated and their energy budget evaluated. The results reveal that free surface scattering has a strong effect on near-source energy partitioning. The scattering process can excite the Rg-wave for a moderately rugged topography but prevents the formation and propagation of short-period Rg-waves when the surface becomes too rugged. For models with a high-velocity shallow crust, the free surface scattering provides an important mechanism that transfers energy for an explosion source into the Lg-wave in the near-source region. At lower frequencies and for a moderately rugged free surface, the Rg-to-Lg transfer is relatively efficient. At higher frequencies and for a very rugged free surface, the body-to-Lg transfer may dominate the process. The correlation length of the random free surface fluctuation provides specific frequency dependence to the transfer function, with maximum coupling near $ka = 1$. Intrinsic attenuation within the uppermost crust has a strong effect on the energy transfer through surface scattering, with high-frequency content losing energy faster than do the lower-frequency waves.

To extend our analysis to the 3D case, we use a 3D finite-difference method that can handle both volumetric heterogeneity and irregular topography. This finite-difference method is ideal for simulating the near-source energy partitioning process. We calculate synthetic seismograms using 3D crust models with different random heterogeneity and random rough-surface parameters. The local slowness analysis method similar to that used in the 2D case is applied to the 3D simulation. We qualitatively investigate the effect of topographic scattering on explosion source energy partitioning in the near-source environment. As preliminary results, the 3D rough free surface causes strong attenuation for the Rg wave. The scattering modifies the energy distribution in the slowness domain and shifts part of the wave energy from small slowness to larger slowness. Apparent SH waves can be seen in scattered waves.

OBJECTIVE

Regional seismic phases (e.g., Pn, Sn, Pg, Lg) play an important role in global monitoring of low-yield underground nuclear tests. Numerous empirical observations have shown that regional phases hold the keys to small-event magnitude and yield estimation and to discrimination between small explosions and earthquakes (e.g., Nuttli, 1986, Taylor et al., 1989; Kim et al., 1993, 1997; Walter et al., 1995; Fisk et al., 1996; Taylor, 1996; Taylor and Hartse, 1997; Hartse et al., 1997; Fan and Lay, 1998a-c; Patton, 2001; Xie, 2002; Bottone et al., 2002). However, building a sound physical basis for the application of the empirical relationships requires detailed knowledge of the regional phases (e.g., relative intensity and frequency dependence of different phases excited by earthquakes and explosions) and relationships linking the wave characteristics with a range of source and structure parameters. The complex excitation and energy partitioning mechanisms yielding regional phases are difficult to empirically separate by data analysis. Thus, numerical modeling approaches are valuable for investigating excitation and propagation of regional seismic phases (e.g., McLaughlin and Jih, 1988; Xie and Lay, 1994; Bradley and Jones, 1998, 1999; Wu, et al. 2000a, b; Bonner, et al., 2003; Stevens et al., 2003; Myers, et al., 2005; Xie, et al., 2005a, b).

Although there are continuing controversies over the relative importance of various energy partitioning mechanisms affecting regional phases, most investigators agree that appreciable S-wave excitation for explosion sources occurs in the near-source region, reducing the performance of event discrimination approaches. Several possible near-source S-wave energy excitation mechanisms have been proposed to explain the generation of explosion Lg-waves. Among these, near-source coupling between P-, S-, and Rg-waves due to scattering at a rugged free surface may play an important role in Lg-wave excitation. This has been investigated by different authors from both observational and theoretical perspectives. From data analysis, Gupta et al. (1992, 2005) suggested that near-source scattering of explosion-generated Rg into S makes a significant contribution to low-frequency Lg signals. With Rg being strongly excited for very shallow explosions relative to deeper earthquakes, efficient Rg-to-Lg scattering often causes the low-frequency P/Lg ratio to fail to discriminate source type. Patton and Taylor (1995) analyzed the Lg spectral ratios from Nevada Test Site (NTS) explosions and suggested that the Lg-wave is generated by near-source scattering of Rg-waves into body waves, which become trapped in the crust. Myers et al. (1999) investigated the 1997 Depth of Burial Experiment at the former Soviet test site at Balapan, Kazakhstan. By comparing the regional and local recordings from explosions at different depths, they suggested that the data support Rg scattering as a major source of explosion S-waves.

Patton and Taylor (1995) introduced theoretical models of the explosion spall source to explain the observed similarity between Rg and Lg spectra. McLaughlin and Jih (1988) used finite-difference simulation to investigate topography influences on teleseismic P-waveforms and indicated possible Rg-to-P scattering due to the near-source topography. More recently, Bonner et al. (2003) and Wu et al. (2003) provided strong evidence in favor of the Rg-to-S scattering mechanism for the generation of the low-frequency S and Lg for explosions. Xie et al. (2005a, b; 2006) investigated the contribution of shallow volumetric scattering and surface scattering to explosion source energy partitioning and calculated the frequency dependent Lg excitation functions. They found that the high-frequency Lg energy is mainly from P-pS-to-Lg and P-to-Lg scattering, while the low-frequency energy is mainly from Rg-to-Lg scattering. Myers et al. (2005), using numerical simulation, investigated the effect of surface topography on the P-to-S conversion. They concluded that near-source topography and geologic complexity in the upper crust strongly contribute to the generation of S-waves.

Given the existence of a rugged free surface, the actual formation and coupling between waves in the near-source region is expected to be rather complex, so it is important to study this phenomenon with the source excitation as part of the model, not simply as a remote propagation effect. Scattering at the rough free surface can change the propagation direction of pP- and pS-waves, causing more of their energy to become trapped in the crustal waveguide and contribute to the Lg-wave than would occur for a flat surface. A rugged free surface and/or shallow heterogeneity also provides coupling between surface waves and body waves. Both body-wave to surface-wave and surface-wave to body-wave scattering can occur. Multiple scattering, variable source depth, and attenuation in the shallow layers are all factors that may affect the frequency-dependent regional wave energy partitioning and these effects need to be quantified.

We report results from both 2D and 3D numerical simulations. For the 2D case, we use a P-SV boundary-element simulation (Ge et al., 2005) and an embedded array slowness analysis method (Xie et al. 2005a) to investigate the effect of topographic scattering on explosion source energy partitioning. Following our last report (Xie, et al. 2006), which covers the effect of rms free surface fluctuation and the intrinsic attenuation on the Lg wave excitation, this report covers the effect of source depth and the correlation length of the rough surface on the energy partitioning. In the 3D case, we use a 3D finite-difference method developed by Zhang and Chen (2006) and the slowness analysis method (Xie et al. 2005a) to investigate the problem. The 3D finite-difference method we adopted can accurately and efficiently implement the traction-free boundary conditions in the presence of an irregular topography. Both the volumetric heterogeneity and the rough free surface can be included in a model. Our preliminary results show that surface and volumetric scattering do cause coupling between the body and surface waves and significantly influence the overall partitioning of explosion energy in the regional wavefield.

RESEARCH ACCOMPLISHED

Energy Partitioning Formalism

For convenience, we symbolically write the near-source energy partitioning process for an explosion source as

$$E^K(p,f) = S(f)R^K(p,f)\,, \tag{1}$$

where $E^K(p,f)$ is the near-source energy partitioned to the type K wave (K can be P, S, Lg, Rg, or other wave types), p is the slowness, f is the frequency, $S(f)$ is the spectrum of an isotropic explosion source. $R^K(p,f)$ is the energy response function of the near source structure for exciting type K wave and can be expressed as

$$R^K(p,f) = R_F^K(p,f) + \sum_J R_F^J(p,f)T^{J\to K}(p,f) - \sum_J R_F^K(p,f)T^{K\to J}(p,f)\,. \tag{2}$$

On the right-hand side of this equation, $R_F^K(p,f)$ is the response of a flat, homogeneous layered earth model, partitioning the source energy into different phases. The transfer function $T^{J\to K}$ provides the J-to-K coupling that modifies the original partitioning by moving energy from one phase to another. The second term on the right-hand side denotes energy being imparted into the K wave through coupling, and the third term denotes energy lost from the K wave to other phases. The combined effect gives the total partitioning of the energy radiated from an isotropic source into the K wave energy distributed in slowness and frequency domains. This energy will develop into different regional phases that propagate to remote distances. Having a complete description of the slowness distribution allows us to accurately predict energy imparted to the distant regional phases based on the near-source energy budget.

The 2D Boundary Element Simulation

Because primary energy partitioning for an explosion source occurs within the near-source region, Xie et al., (2005a) developed a slowness analysis method that can be applied for full wavefield computations to separate the problem into consideration of near-source energy partitioning effects apart from long-range propagation effects. A localized slowness analysis for an array embedded in the numerical calculation tracks the energy partitioning occurring close to the source, replacing an expensive long-distance propagation calculation. Xie et al. (2005a) demonstrated that the energy partitioning from the near-source slowness analysis accurately predicts the energy distribution for surface observations at large range. The method has two major advantages. First, it allows analysis of the near-source processes in multiple domains, including space, time, slowness, and frequency. This allows isolation of different excitation and partitioning mechanisms within the complex near-source environment. Second, the embedded array slowness analysis method can be applied at a close range, well before the Lg-wave is actually formed. This allows numerous simulations for a relatively small-scale velocity model with very fine near-source structures. We use a 2D P-SV wave boundary-element method (Ge et al., 2005) to generate synthetics seismograms for an explosion source. The boundary element method has been proved to be an accurate wave propagation approach when the earth model includes irregular surfaces.

Space domain representation of surface scattering

Illustrated in Figure 1 are boundary element generated snapshots for wavefields in a model with free surface scattering. A random fluctuation with a correlation length of 0.5 km and an rms fluctuation of 0.15 km is used for the free surface and extends between distances 30 and 50 km. The source is located at distance of 20 km and a depth of 0.5 km. Figures 1a and 1b are horizontal and vertical displacements. In addition to familiar major phases (e.g., *P*, *pS*, *Rg*) expected for a shallow explosion in a flat earth model, scattered body and surface waves from the rough free surface are present in the wavefield. The surface-to-body and body-to-body wave scattering is distributed through the entire medium following the primary waves, and the body-to-surface and surface-to-surface wave scattering is concentrated at very shallow depths following primary waves as they graze the surface.

To isolate the scattered phases, we subtract the wavefield generated for a flat surface from the wavefield for the model having a rough surface, yielding the results presented in Figures 1c and 1d. Most of the scattered body waves are shear waves. Due to the coupling between different wave numbers, the scattered body waves have a very broad range of propagation directions.

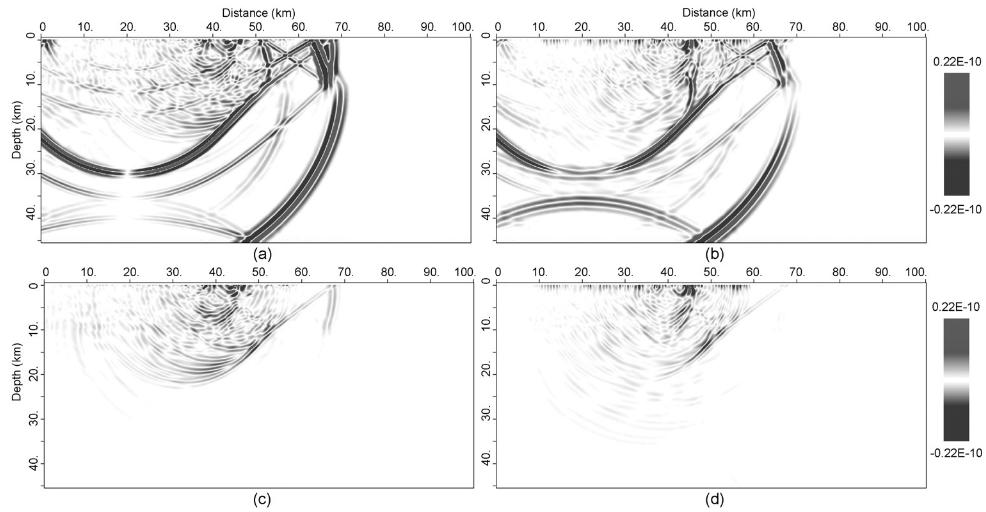

Figure 1. Wavefield snapshot at t = 10.0 s for a model with random free surface fluctuation, where (a) and (b) are horizontal and vertical components of the wavefield and (c) and (d) are horizontal and vertical components of the scattered wavefield obtained by subtracting the flat model wavefield from the random surface wavefield. The source is at 20 km horizontal position and 0.5 km depth.

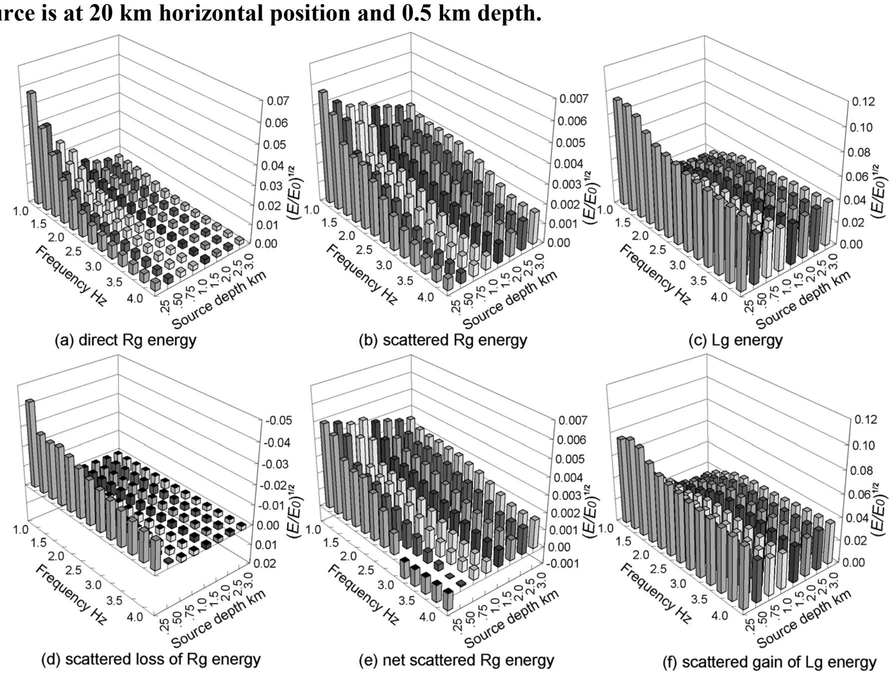

Figure 2. Responses as functions of frequencies and source depths. Top row: the near-source responses of direct *Rg*, scattered *R,g* and the *Lg*-waves, with (a) R^{Rg_direct}, (b) R^{Rg_scatt} and (c) R^{Lg}. Bottom row: the contributions of surface scattering to these responses, with (d) $R^{Rg\_direct} - R_F^{Rg\_direct}$, (e) $R^{Rg\_scatt} - R_F^{Rg\_scatt}$ and (f) $R^{Lg} - R_F^{Lg}$. Note, a negative vertical coordinate is used in (d).

The effect of source depth

We adopt a three-layer crust as our basic velocity model and add random free surface fluctuations with different statistical parameters to this basic model. The random topography has an exponential power spectrum. It is located above the source and extends in both directions for 20 km. To characterize the results statistically, we generate 10 realizations for each model. Synthetic seismograms are calculated for each realization and processed separately. We then average the measurements from individual realizations and use their mean value as the final result for a particular case.

To investigate the effect of source depth on the energy partitioning, we fix the rms free surface fluctuation at 0.15 km and the correlation length as 0.5 km and vary the source depth between 0.25 km and 3.0 km. Figures 2a to 2c present the response functions of direct *Rg*- , scattered *Rg*-, and *Lg*-waves with respect to frequencies and source depths. With increasing source depth, the *Rg* energy falls quickly. Shown in Figures 2d to 2f are separated net contributions from the free surface scattering obtained by subtracting the energy of the flat earth model from that for a random free surface. For direct *Rg* from a shallow source, a large amount of energy is lost due to scattering. However, for deeper sources, the scattering adds a small amount of energy to the *Rg*-wave. The scattered *Lg*-wave shows an apparent increase for sources shallower than about 0.5 km, which suggests a surface wave origin. The energy budget between Figures 2d and 2f is also comparable at lower frequencies. For *Lg*-wave with frequencies of 3 Hz or higher, the energy should come from body wave surface scattering. For deeper sources, the lower-frequency *Lg*-wave is very weak, indicating that both *Rg*-to-*Lg* and body-to-*Lg* conversions are weak within this frequency-depth range.

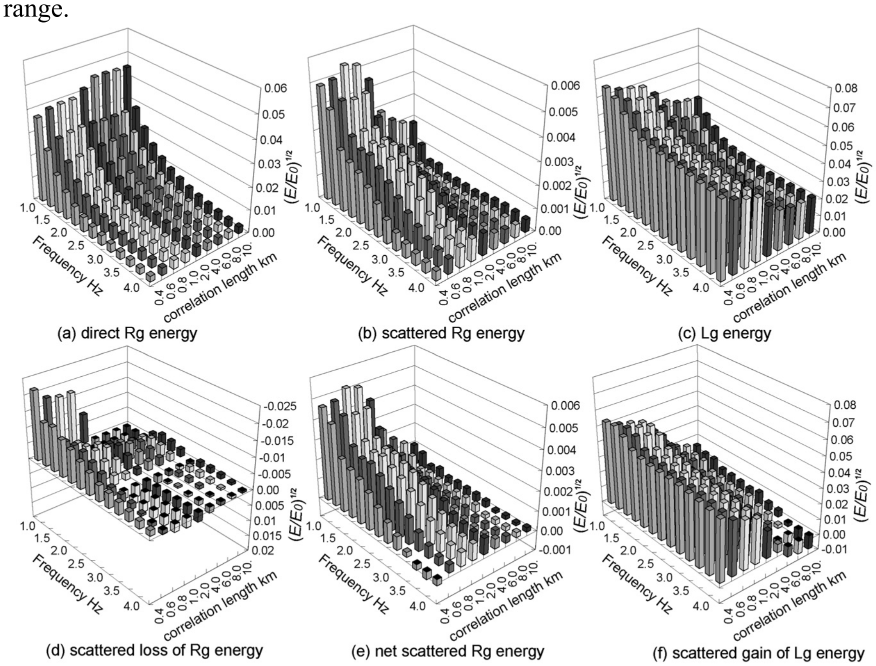

Figure 3. Similar to Figure 2, except responses are functions of frequencies and correlation lengths.

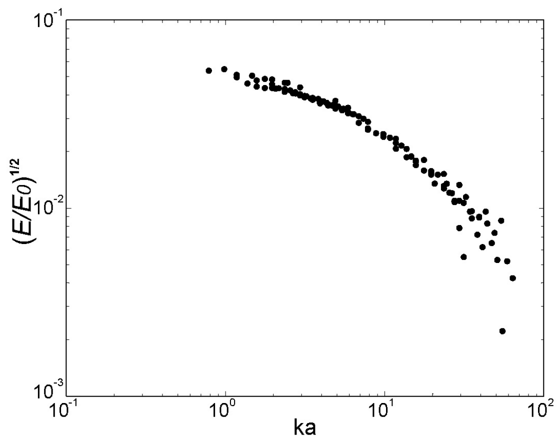

Figure 4. Net scattered Lg-energy as a function of normalized scale factor *ka*.

The effect of correlation length

To investigate the effect of correlation length on the energy partitioning, we fix the rms free surface fluctuation as 0.15 km and the source depth at 0.5 km and vary the correlation length between 0.4 km and 10 km. The response functions of *Rg*-, scattered *Rg*- and *Lg*-waves are shown in Figures 3a to 3c. The horizontal coordinate is frequency, and different rows are for different correlation lengths. From these response functions, we see that the last row (for a correlation length of 10 km) is almost the same as that for a flat earth model. This indicates that a very smooth long wavelength free surface fluctuation has almost no effect on these waves.

In Figure 3f, the net scattered contribution to the *Lg*-wave, the response function falls with increases of the correlation length at all frequencies. For frequencies used in the simulation (1 to 4 Hz) and *S*-wave velocity in the top layer (3.2 km/sec), the wavelengths are between 0.8 and 3.2 km. We calculate the response as a function of normalized scale length, ka , where $k = 2\pi/\lambda$, λ is the wave length and *a* is the correlation length, and present the behavior in Figure 4. The maximum scattering happens around $ka = 1$ and decreases for larger ka . Extension of the calculation to smaller ka is limited by the grid size used in the boundary element calculation and the dimension of the receiver array.

The 3D Finite-Difference Simulation

To include both volumetric heterogeneity and irregular topography in a 3D simulation and investigate their effects on near-source energy partitioning, we use the 3D finite-difference method developed by Zhang and Chen (2006). In this finite-difference algorithm, the physical domain is discretized by boundary-conforming grids. The irregular surface is transformed into a “flat” surface in computational space, thus avoiding the artifact usually caused by using the staircase approximation. To satisfy the free surface boundary conditions, the method uses the stress image method on the irregular topography. With this method, approximately 10 grid points per shortest wavelength are usually enough to maintain the global accuracy of the simulation. Shown in Figure 5 is the velocity model geometry used in near-source simulations throughout this report. The size of the model is $60\,\mathrm{km}\times 60\,\mathrm{km}\times 30\,\mathrm{km}$, with a grid size of $600\times 600\times 300$. An explosion source is located at the center of the model with a depth of 0.5 km. The rough topography is located between epicenter distances 5 and 15 km. The volumetric heterogeneity is located between horizontal distances 5 and 15 km and between depths 1 km and 5 km. A $N_x \times N_y \times N_z = 10\times 10\times 16$ ($4\,\mathrm{km}\times 4\,\mathrm{km}\times 30\,\mathrm{km}$) receiver array located at epicenter distance 28 km is used to collect the synthetic seismograms.

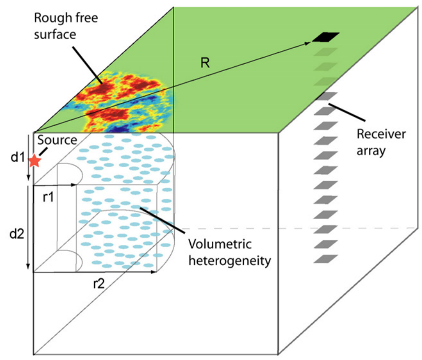

Figure 5. The 3D velocity model, including both irregular free surface and volumetric heterogeneity. The rough topography is located between distances 5 km and 15 km. The volumetric heterogeneity is located between distances 5 km and 15 km and between depths 1 km and 5 km. The synthetic seismograms are collected from a 3D array. Shown in the figure is one quarter of the model.

Shown in Figure 6 are snapshots for an explosion source in different velocity models. Rows (a) to (d) are for a layered model, a layered model with volumetric random velocity fluctuation, a layered model with irregular topography, and a layered model with both volumetric heterogeneity and random topography. The three columns are for x-, y- and z-components. The model geometry is shown in Figure 5. The rough surface has an exponential power spectrum, an rms fluctuation of 0.2 km, and a correlation distance of 2.0 km. The volumetric heterogeneity has an exponential power spectrum, an rms perturbation of 5%, and a correlation length of 2.0 km. For a layered model [row (a)], an explosion source generates P, pS, Rg, and some interface reflections, which are all P-SV waves. As examples, we see the x-component is zero in plane *yOz*, and y-component is zero in plane *xOz*. For models with volumetric and/or rough topography [rows (b) to (d)], there are appearent scattered waves following the primary phases. Particularly, SH-waves appear in the tangential component, e.g., the non-zero x-component in *yOz* plane and the non-zero y-component in *xOz* plane.

Shown in Figure 7 are synthetic seismograms for models with different free surfaces. The model geometry is shown in Figure 5. The top, middle, and bottom rows are for radius, tangential, and vertical components, respectively. Column (a) is for a layered crust model with a flat free surface. Column (b) is for a layered model with a rough topography that has a Gaussian power spectrum, an rms fluctuation of 0.1 km, and a correlation length of 2.0 km. The column (c) is similar to (b), except the random power spectrum is exponential. The results show that the rough topography strongly attenuates the surface wave and generates scattered SH waves.

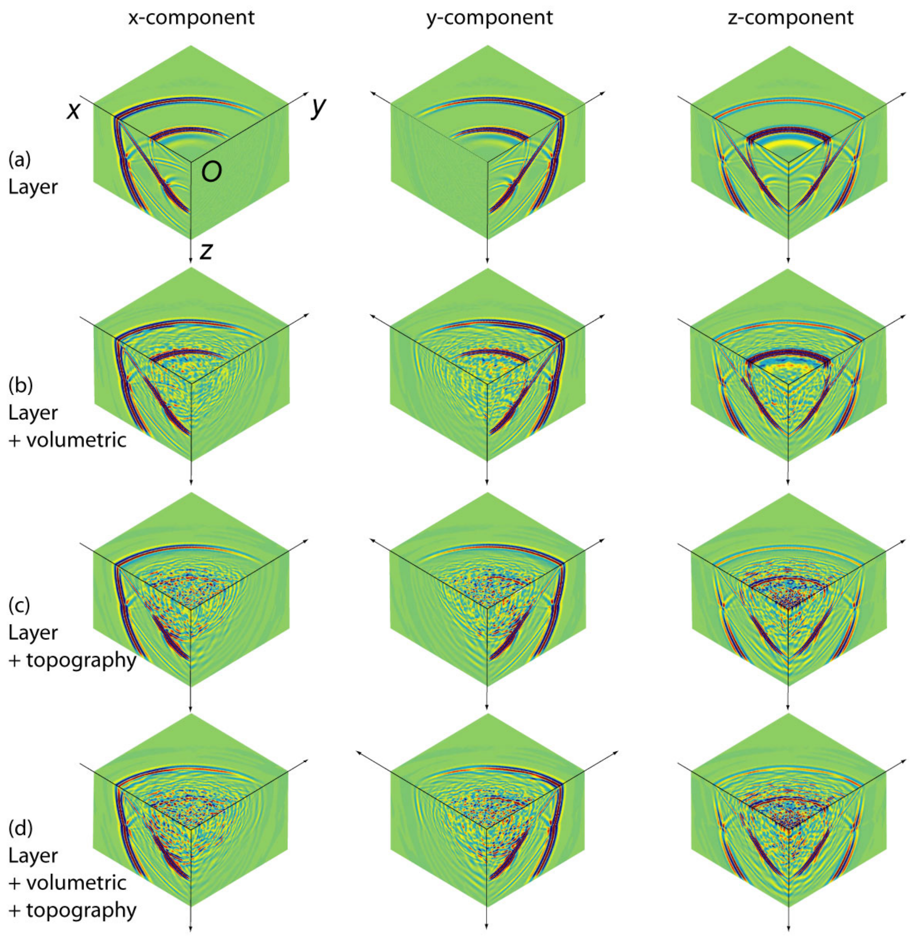

Figure 6. Snap shots for an explosion source in different velocity models. Rows (a) to (d) are for a layered model, a layered model with volumetric random velocity fluctuation, a layered model with irregular topography, and a layered model with both volumetric heterogeneity and random topography. The three columns are for x-, y- and z-components.

Shown in Figure 8 are synthetic seismograms and slowness analysis for (a) a layered crustal model and (b) a layered model with both rough free surface and volumetric heterogeneity. The model geometry is shown in Figure 5. The top, middle, and bottom rows are for radius, tangential, and vertical components, respectively. The rough surface has an exponential power spectrum, an rms fluctuation of 0.2 km and a correlation distance of 2.0 km. The volume heterogeneity has a 5% velocity perturbation, an exponential power spectrum, and a correlation length of 2 km. The synthetic seismograms are filtered between 0.5 and 5.0 Hz, and normalized using the same scale. The horizontal distance from the source to the center of the receiver array is about 28 km. The 2D slowness analyses are conducted in horizontal plane (the map view) with these panels roughly correspond to P, PP, PS, Rg, and coda waves. The results show that for an explosion source in a layered model, there is no SH wave and the energy is distributed within the upper mantle S-wave slowness (the dashed circle). For a model with rough free surface and the volumetric heterogeneity, the primary P and Rg waves are strongly attenuated due to the scattering. From slowness analysis, there are both SV and SH energy with their slowness distributed outside of the upper mantle S-wave slowness, indicating part of their energy to become trapped in the crustal waveguide to contribute to the *Lg*-wave.

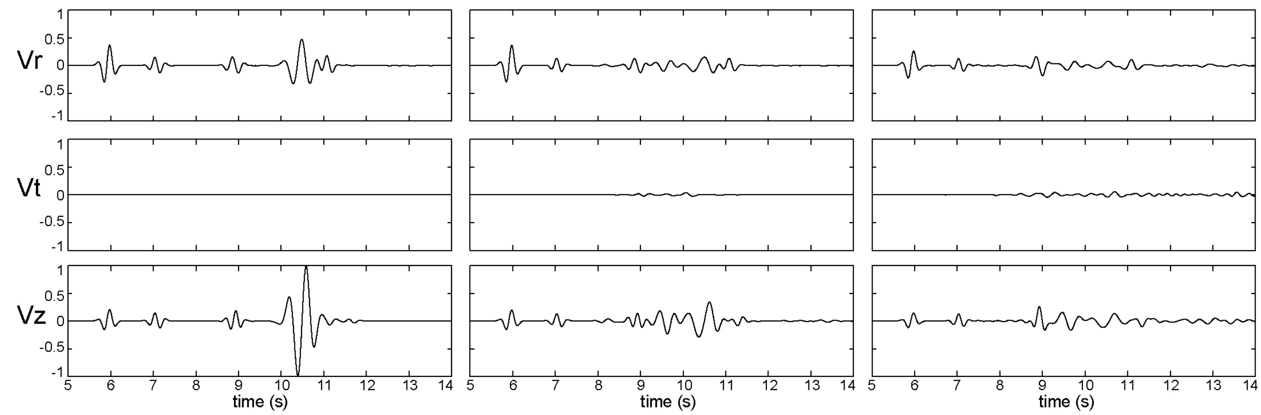

(a) (b) (c)

Figure 7. Synthetic seismograms for (a) a layered crust model with flat free surface, (b) a layered model with Gaussian rough free surface, and (c) a layered model with exponential rough free surface. All seismograms are normalized with the same scale.

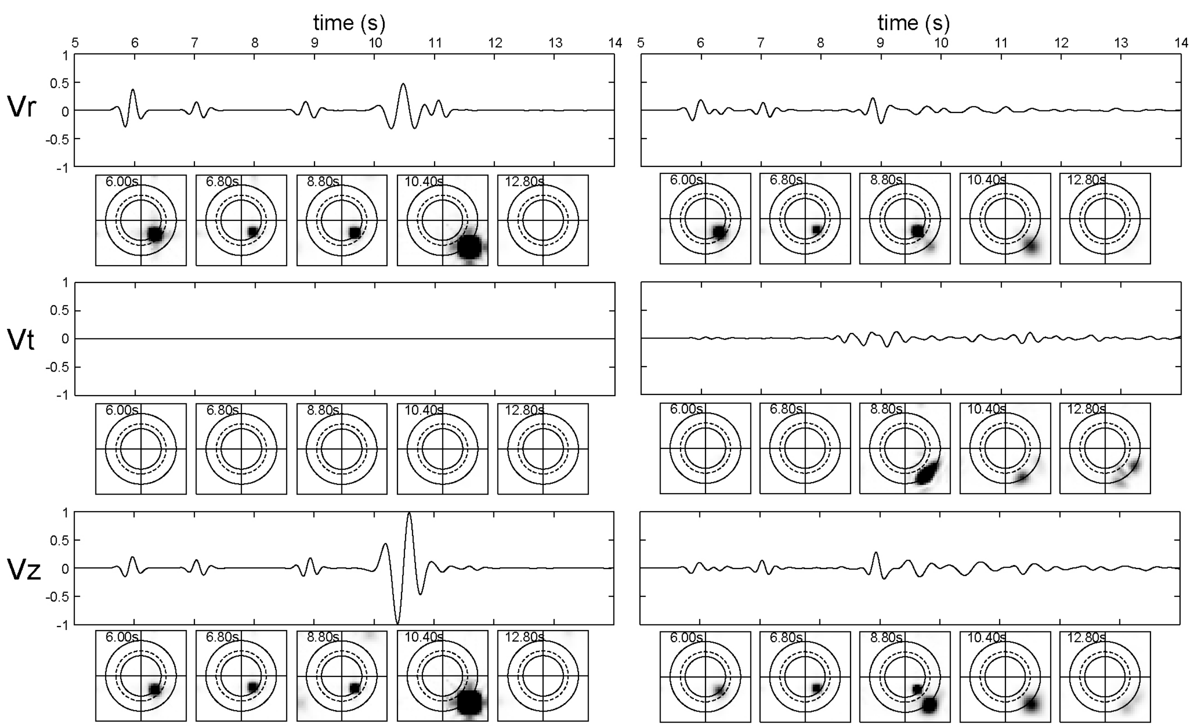

(a) (b)

Figure 8. Synthetic seismograms and slowness analysis for a layered crustal model [column (a)] and a layered model with both rough free surface and volumetric heterogeneity [column (b)]. The model geometry is shown in Figure 5.

<u>CONCLUSIONS AND RECOMMENDATIONS</u>

We use the 2D P-SV boundary-element simulation and the embedded array local slowness analysis method to investigate the effect of topographic scattering on the near-source energy partitioning for an explosion source. Random topographic models with different statistical properties, variable source depth, and different Q models are investigated using numerical simulations. The responses of different phases as functions of frequency and source/model parameters are calculated and their energy budget evaluated. The results reveal that free surface scattering has a strong effect on near-source energy partitioning. However, in many cases, the scattering in 2D geometry may not be the same as in the real 3D world. We expand our analysis to fully 3D models with both volumetric heterogeneity and rough free surface. The preliminary result included in this report is promising. A series of analyses similar to what we applied to the 2D model will be conducted to the 3D model. Both the volume scattering and the free surface scattering will be judged for their roles in the near-source energy partitioning.

ACKNOWLEDGEMENT

The authors wish to thank Dr. Wei Zhang for kindly providing us with his 3D finite-difference code.

REFERENCES

Bonner, J. B., H. J. Patton, A. C. Rosca, H. Hooper, J. Orrey, M. Leidig and I. Gupta (2003). Aspects of *Rg* and *Lg* generation from the Shagan depth of burial explosions, in *Proceedings of the 25th Seismic Research Review—Nuclear Explosion Monitoring: Building the Knowledge Base*, LA-UR-03-6029, Vol. 1, pp. 384–394.

Bottone, S., M. D. Fisk, and G. D. McCartor (2002). Regional seismic event characterization using a Bayesian formulation of simple kriging, *Bull. Seism. Soc. Am*. 92: 2277–2296.

Bradley, C. R., and E. M. Jones (1998). Modeling propagation effects from explosion in Western China and India, in *Proceedings of the 20th Annual Seismic Research Symposium on Monitoring a Comprehensive Nuclear-Test-Ban Treaty*, Santa Fe, New Mexico, September 21–23.1998, pp. 173–181.

Bradley, C. R., and L. E. Jones (1999). Full waveform modeling of the effects of Q and structure over sub-regional paths, in western China, in *Proceedings of the 21st Annual Seismic Research Symposium on Monitoring a Comprehensive Nuclear-Test-Ban Treaty*, Las Vegas, Nevada, 21-24 September 1999, 28-38.

Fan, G. W., and T. Lay (1998a). Statistical analysis of irregular waveguide influences on regional seismic discriminants in China, *Bull. Seism. Soc. Am*. 88: 74–88.

Fan, G. W., and T. Lay (1998b). Regionalized versus single-station wave-guide effects on seismic discriminants in western China, *Bull. Seism. Soc. Am*. 88: 1260–1274.

Fan, G. W., and T. Lay (1998c). Statistical analysis of irregular waveguide influences on regional seismic discriminants in China: additional results for *Pn*/*Sn*, *Pn*/*Lg* and *Pg*/*Sn*, *Bull. Seism. Soc. Am*. 88: 1504–1510.

Fisk, M. D., H. L. Gray, and G. D. McCartor (1996). Regional discrimination without transporting thresholds, *Bull. Seism. Soc. Am*. 86: 1545–1558.

Ge, Z., L. Y. Fu and R. S. Wu (2005). *P-SV* Wavefield connection technique for regional wave propagation simulation, *Bull. Seism. Soc. Am.* 95 1375–1386.

Gupta, I. N., W. W. Chan, and R. A. Wagner (1992). A comparison of regional phases from underground nuclear explosions at East Kazakh and Nevada Test Sites, *Bull. Seism. Soc. Am*. 82, 352-382.

Gupta, I. N., W. W. Chan, and R. A. Wagner (2005). Regional source discrimination of small events based on the use of *Lg* wavetrain, *Bull. Seism. Soc. Am*. 95: 341–346.

Hartse, H. E., S. R. Taylor, W. S. Phillips, and G. E. Randall (1997). A preliminary study of regional seismic discrimination in central Asia with emphasis on western China, *Bull. Seism. Soc. Am*. 87: 551–568.

Kim, W. Y., V. Aharonian, A. L. Lerner-Lam, and P. G. Richards (1997). Discrimination of earthquakes and explosions in southern Russia using regional high-frequency three-component data from IRIS/JSP Caucasus Network, *Bull. Seism. Soc. Am*. 87: 569–588.

Kim, W. Y., D. W. Simpson, and P. G. Richards (1993). Discrimination of earthquakes and explosions in the eastern United States using regional high-frequency data, *Geophys. Res. Lett*. 20: 1507–1510.

McLaughlin, K. L., and R. S. Jih (1988). Scattering from near-source topography: Teleseismic observations and numerical simulations, *Bull. Seism. Soc. Am*. 78: 1399–1414.

Myers, S. C., W. R. Walter, K. Mayeda, and L. Glenn (1999). Observations in support of *Rg* scattering as a source for explosion *S* waves: Regional and local recordings of the 1997 Kazakhstan depth of burial experiment, *Bull. Seism. Soc. Am*. 89: 544–549.

Myers, S. C., J. Wagoner, L. Preston, K. Smith, and S. Larsen (2005). The effect of realistic geologic heterogeneity on local and regional *P*/*S* amplitude ratios based on numerical simulations, in *Proceedings of the 27th Seismic Research Review: Ground-Based Nuclear Explosion Monitoring Technologies*, LA-UR-05-6407, Vol. 1, pp. 123–132.

Nuttli, O. W. (1986). Yield estimates of Nevada Test Site explosions obtained from *Lg* waves, *J. Geophys. Res*. 91: 2137–2151.

Patton, H. J. (2001). Regional magnitude scaling, transportability, and Ms:mb discrimination at small magnitudes, *Pure appl. Geophys*. 158: 1951–2015.

Patton, H. J., and S. R. Taylor (1995). Analysis of *Lg* spectral ratios from NTS explosions: implications for the source mechanisms of spall and the generation of *Lg* waves, *Bull. Seism. Soc. Am*. 85: 220–236.

Stevens, J. L., G. E. Baker, H. Xu, T. J. Bennett, N. Rimer, and S. M. Day (2003). The physical basis of *Lg* generation by explosion sources, in *Proceedings of the 25th Seismic Research Review, Nuclear Explosion Monitoring: Building the Knowledge Base*, LA-UR-03-6029, Vol. 1, pp. 456–465.

Taylor, S. R. (1996). Analysis of high frequency *Pn*/*Lg* ratios from NTS explosions and western U.S. earthquakes, *Bull. Seism. Soc. Am*. 86, 1042–1053.

Taylor, S. R., M. D. Denny, E. S. Vergino, and R. E. Glaser (1989). Regional discrimination between NTS explosions and western U.S. earthquakes, *Bull. Seism. Soc. Am*. 79: 1142–1176.

Taylor, S. R. and H. E. Hartse (1997). An evaluation of generalized likelihood ratio outlier detection to identification of seismic events in Western China, *Bull. Seism. Soc. Am*. 87: 824–831.

Walter, W. R., K. M. Mayeda, and H. Patton (1995). Phase and spectral ratio discrimination between NTS earthquakes and explosions, Part I: Empirical observations, *Bull. Seism. Soc. Am.* 85: 1050–1067.

Wu, R. S., S. Jin and X. B. Xie (2000a). Seismic wave propagation and scattering in heterogeneous crustal waveguides using screen propagators: I *SH* waves, *Bull. Seism. Soc. Am*. 90: 401–413.

Wu, R. S., S. Jin and X. B. Xie (2000b). Energy partition and attenuation of *Lg* waves by numerical simulations using screen propagators, *Phys. Earth and Planet. Inter*. 120: 227–243.

Wu, R. S., X. B. Xie, Z. Ge, X. Wu, and T. Lay (2003). Quantifying source excitation and path effects for high-frequency regional waves, in *Proceedings of the 25th Seismic Research Review, Nuclear Explosion Monitoring: Building the Knowledge Base*, LA-UR-03-6029, Vol. 1, pp. 172–181.

Xie, J. (2002). Source scaling of *Pn* and *Lg* spectra and their ratios from explosions in central Asia: Implications for the identification of small seismic events at regional distances, *J. Geophys. Res*. 107: B7, 10.1029/2001JB000509.

Xie, X. B. and T. Lay (1994). The excitation of *Lg* waves by explosions: A finite-difference investigation, *Bull. Seism. Soc. Am*. 84: 324–342.

Xie, X. B., Z. Ge and T. Lay (2005a). Investigating explosion source energy partitioning and *Lg*-wave excitation using a finite-Difference plus slowness analysis method, *Bull. Seism. Soc. Am*. 95: 2412–2427.

Xie, X. B., T. Lay, and R. S. Wu (2005b). Near source energy partitioning for regional waves in 2D and 3D models, contributions of *S**-to-*Lg* and *P*-to-*Lg* scattering, in *Proceedings of the 27th Seismic Research Review: Ground-based Nuclear Explosion Monitoring Technologies*, LA-UR-05-6407, Vol. 1, pp. 249–258.

Xie, X. B., T. Lay, R. S. Wu and Y. He (2006). Near source energy partitioning for regional waves in 2D and 3D models, contributions of free surface scattering, in *Proceedings of the 28th Seismic Research Review: Ground-based Nuclear Explosion Monitoring Technologies*, LA-UR-06-5471, Vol. 1, pp. 304–314.

Zhang, W., and X. Chen (2006). Traction image method for irregular free surface boundaries in finite difference seismic wave simulation, Geophys. J. Int. 167: 337–353.